Synthesis Imaging in Radio Astronomy II
ASP Conference Series, Vol. XXX, 1998
G.B. Taylor, C.L. Carilli, and R. A. Perley (eds.)

Space Very Long Baseline Interferometry

J.S. Ulvestad
National Radio Astronomy Observatory, Socorro, NM, USA, 87801

Abstract. Space Very Long Baseline Interferometry (SVLBI) is a technique in which an array of ground radio telescopes observes a source in conjunction with one or more orbiting radio telescopes. A synthesized aperture is produced with a diameter approximately equal to the apogee of the spacecraft orbit, enabling higher resolution imaging than is possible with ground-only VLBI. This paper discusses the characteristics and techniques of SVLBI, emphasizing the differences in capabilities and data-processing from traditional VLBI. General concepts are illustrated with a number of examples from the currently operational VLBI Space Observatory Programme, using a dedicated SVLBI satellite that was launched in February 1997.

1 Introduction

Space Very Long Baseline Interferometry (hereafter SVLBI) is a technique that is used to extend the maximum baseline available in VLBI observations. This is done by launching a radio telescope into space, preferably in an elliptical orbit around the Earth. The SVLBI satellite then observes in conjunction with ground radio telescopes, synthesizing an aperture whose effective resolution is that of a radio telescope much larger than the Earth. This enables imaging of the most compact radio sources in the universe with sub-milliarcsecond resolution.

The first SVLBI demonstrations were carried out from 1986 through 1988 (Levy et al. 1986, 1989; Linfield et al. 1990), using an element of NASA's Tracking and Data Relay Satellite System (TDRSS). A 4.9-meter radio antenna aboard a geostationary satellite above the western Atlantic Ocean was used as the orbiting telescope. Successful observations were carried out at observing frequencies of 2.3 and 15 GHz, demonstrating that there were no insurmountable technical obstacles to scientific observations with a dedicated SVLBI satellite. In the most extensive series of observations, carried out in early 1987, a number of sources were shown directly to have apparent rest-frame brightness temperatures in excess of 10^{12} K (Linfield et al. 1989).

The success of the original demonstrations was an important argument for the proposed QUASAT (Schilizzi et al. 1984) and IVS (International VLBI Satellite; see Pilbratt 1991) concepts, neither of which was ultimately approved. However, the TDRSS demonstrations led to development of the HALCA (Highly Advanced Laboratory for Communications and Astronomy) satellite of the VLBI Space Observatory Programme (VSOP). HALCA was developed by the Institute of Space and Astronautical Science (ISAS) in Japan, and launched in February 1997. It carries an 8-meter radio telescope that works with ground telescopes to image radio sources at 1.6 and 5 GHz (see Hirosawa & Hirabayashi 1995; Hirabayashi 1998; Hirabayashi et al. 1998). VSOP is used for many examples in this article; more details can be found in the VSOP Proposer's Guide (VSOP Science Operations Group 1998). Another mission, RadioAstron (Kardashev 1997), awaits a launch some time after the turn of the century.

2 Orbit Influence on (u,v) Coverage

The primary purpose of doing SVLBI is to increase the maximum baseline length sampled in a given observation. However, baselines that are too long relative to the ground baselines can give large holes in the (u,v) plane, leading to significant imaging defects. Furthermore, evolution of the orbit parameters leads to changes in the (u,v) coverage over time scales of months, having a significant impact on observation planning. This section discusses some of the effects of the orbit on SVLBI observations.

2.1 Orbit Parameterization

Typically, a spacecraft orbit is defined by six fundamental parameters (see Bate, Mueller, & White 1971, p. 59, for a useful sketch):

- a = semi-major axis of the orbit.
- e = orbital eccentricity.
- i = inclination with respect to the Earth's equator.
- Ω = longitude of the ascending node. This is the angle in the Earth's equatorial plane, in the same sense as the motion of the satellite, from the direction of the vernal equinox to the ascending node. The ascending node is the intersection of the equatorial plane with the satellite's orbital plane, at the location where the satellite moves north of the equator.
- ω = argument of perigee. This is the angular distance from the ascending node, along the orbit plane, to the direction of perigee.
- T = time of the satellite's perigee passage.

The location of the satellite at a particular time is often represented by the mean anomaly, M. This gives the fraction of an orbital period (often expressed in degrees) traversed since the last perigee passage. For example, for a spacecraft in an orbit with an 8-hr period, which passes perigee at 02:00 UT, $M = 135°$ at 05:00 UT and $M = 180°$ at 14:00 UT.

2.2 Orbit Selection

Selection of an orbit is akin to choosing the locations of the telescopes in design of a synthesis array such as the VLA or the VLBA (e.g., Walker 1984). One might think that the top priority is to launch the spacecraft into the highest possible orbit. However, very high orbits have several disadvantages. First, large holes are created in the (u,v) plane, limiting the dynamic range of images. Second, the orbit size should be scaled to the size of the physical phenomena of interest. If the orbit is too high, source brightnesses may be too low for detection, or sources may vary during a single orbit (a suitable imaging interval). Third, launch vehicles are usually a substantial fraction (10%–30%) of the overall mission cost of hundreds of millions of dollars, so budget limitations constrain the apogee height. Finally, for fixed properties of the data transmission system, the maximum downlink data rate (hence observing bandwidth) is reduced according

to the inverse-square law. If the orbit is too high, the correlated flux will drop and the observing bandwidth must be decreased, seriously degrading the signal-to-noise ratio for fringe detection.

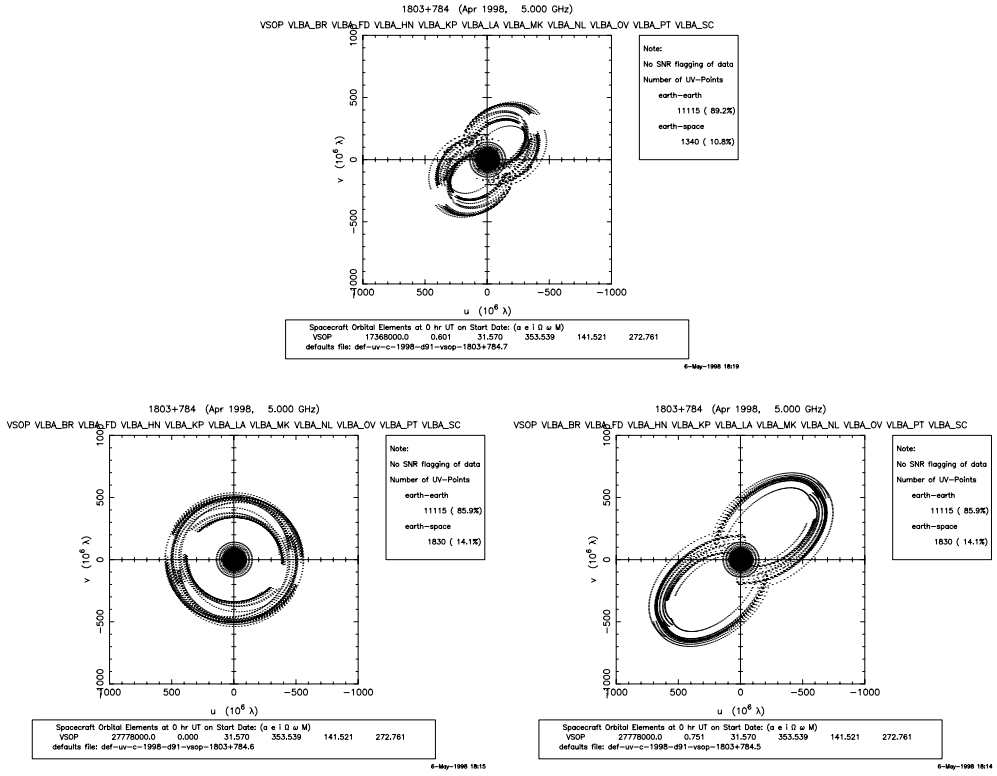

Figure 1. Sample 5-GHz SVLBI (u,v) coverages for 24-hr (spacecraft + VLBA) observations of the quasar 1803+784 on 1 April 1998. All plots are at the same scale, from 10^{-9} to 10^{9} wavelengths in u and v. *Top:* HALCA orbit. *Lower left:* Circular orbit with height equal to HALCA apogee height. *Lower right:* Highly elliptical orbit with semi-major axis equal to the radius of the circular orbit in the lower left panel.

Figure 1 illustrates some simple consequences of orbit selection for a hypothetical 24-hr observation of the northern quasar 1803+784 on 1 April 1998, as simulated using FAKESAT (Murphy et al. 1994; Murphy 1995). The top panel shows the (u,v) coverage for an observation using the VLBA with HALCA, whose orbital elements on that date were $(a, e, i, \Omega, \omega, T)$ = (17,368 km, 0.601, 31.57°, 353.4°, 141.5°, 01:32 UT on 1998 April 1). This elliptical orbit has an apogee height of 21,400 km, a perigee height of 540 km, and a 6.3-hr period. The lower left panel shows the (u,v) coverage for a circular orbit with a height of 21,400 km. This orbit has $a = 27,778$ km and $e = 0$ (12.8-hr period). The maximum baseline length is similar to that for HALCA, but there is a large gap between the ground baselines and the longer space-ground baselines. Finally, the lower right panel shows the coverage for a larger elliptical orbit, also having $a = 27,778$ km and a 12.8-hr period. Here, the perigee height is the same as HALCA, 540 km, but the apogee height is 42,300 km, and $e = 0.751$. For this orbit, the longest baseline has been increased considerably, and the shortest

ground-space baselines overlap the ground-ground baselines, but the size of the holes in the (u,v) plane is quite large.

2.3 Variations in u and v During Observation

The imaging of interferometry data is done by gridding the sampled visibilities onto the (u,v) plane and then Fourier transforming them to create an image (Sramek & Schwab 1989; Briggs 1998). The classic problem of time-average smearing is caused by assigning values of u and v corresponding to the midpoint of an averaging interval, when they actually vary throughout that interval (see Bridle & Schwab 1989). Since correlator integration times are usually about a second, and SVLBI fields of view are generally small, time-average smearing is avoidable unless the data set must be averaged to make computations practical. (For details, see VSOP Science Operations Group 1998, p. 25.)

A related problem is caused by the $\sim$ 10 km s^{-1} spacecraft speed near perigee, combined with the fact that the projected space-ground baselines may be as short as $\sim$ 1000 km at the same time. Integration times of hundreds of seconds often are required to detect fringes to the spacecraft. This implies that u and v can double during a fringe-fit interval, so the structure phase in the visibility function may change substantially, causing a loss of coherence (and signal-to-noise ratio) in the fringe fit on time scales longer than tens of seconds. The effect is much smaller near apogee, since u and v are considerably larger, and the spacecraft is moving only $\sim$1–3 km s^{-1}.

2.4 Orbit Effects on (u,v) Coverage in Different Directions

The resolution of an interferometer depends on its baseline length projected on the plane normal to the source direction. In SVLBI, the longest baselines lie in the spacecraft orbit plane. Therefore, the best two-dimensional (u,v) coverage will occur for sources lying in directions near the normal to the orbit plane, while the coverage for sources near that plane will be extremely elongated. To illustrate this point, Figure 2 is a FAKESAT (Murphy 1995) plot of the (u,v) coverage as a function of position on the sky for 24-hr observations made with HALCA and the VLBA, on 1 April 1998. For simplicity, and to illustrate the basic points, all observing constraints, including the Sun-avoidance angle (see Section 3.6), have been neglected. In the figure, the sinusoidal line with an amplitude of 31.6° is the plane of the spacecraft orbit, P and A indicate the perigee and apogee directions, respectively, and N represents the two normals to the orbit plane. (A Sun angle of 70° also is shown by the curved lines centered on the Sun location.) Inspection of the figure shows that the (u,v) coverage is basically one-dimensional near the orbit plane and two-dimensional near the orbit normals, and that the lengths of the projected baselines are shortest for sources in the directions near apogee and perigee. Sources in the far south are not visible to the VLBA, so there is no (u,v) coverage at $-80°$ declination.

2.5 Effects of Orbit Precession on (u,v) Coverage at Different Times

In Figure 2, equatorial sources near 12 hours right ascension have (u,v) coverage that is quite one-dimensional. Two very important VLBI sources, 3C 273 and 3C 279, are in this vicinity, so it seems that VSOP would be a poor imaging mission for these quasars. However, the geometry changes because of the Earth's

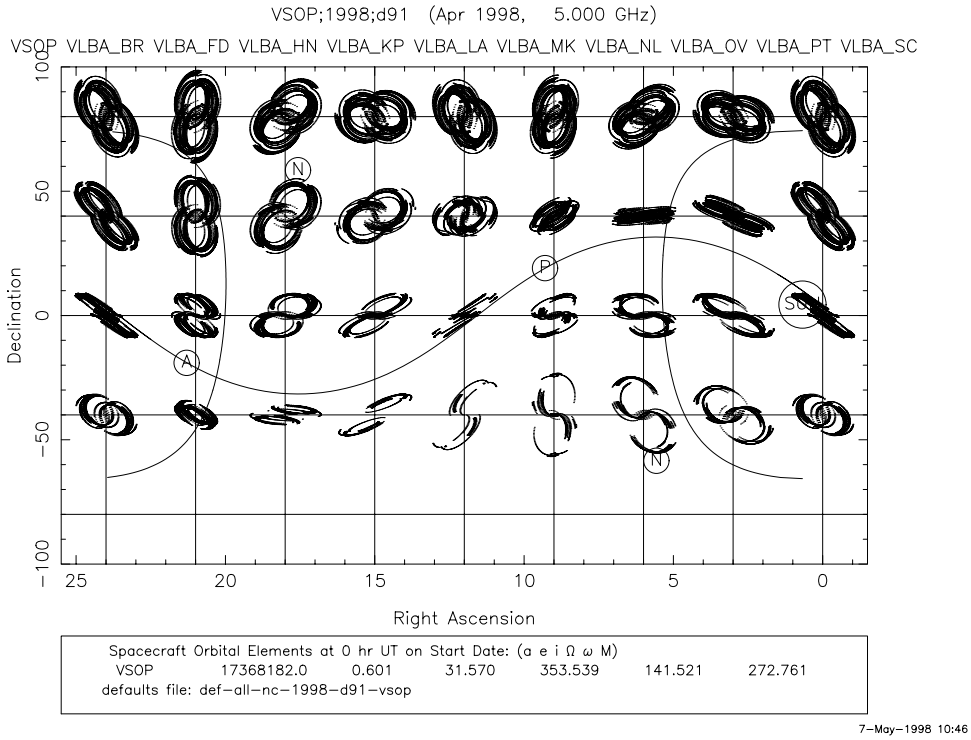

Figure 2. 5-GHz SVLBI (u,v) coverages as a function of sky position, for HALCA+VLBA, on 1 April 1998. No HALCA observing constraints are included other than the requirement that there be a line of sight between the spacecraft and a tracking station.

oblateness, particularly the J_2 term in the Earth's gravitational potential, which causes both Ω and ω to precess. (Precession caused by the Moon and Sun are generally negligible, by comparison.) This changes both the orientation of the orbit plane and the location of perigee within that plane. Thus, precession improves the (u,v) coverage for a given source at some epochs, but the non-repeating coverages make the interpretation of monitoring observations much more difficult.

The equations for the rates of precession can be found in many references (e.g., Griffin & French 1991; Boden 1992); the precession rates due to J_2 are

$$\dot{\Omega}(J_2) = -2.065\ (a/10{,}000\ \mathrm{km})^{-7/2}\ (\cos i)(1-e^2)^{-2}\ \mathrm{deg/day} \qquad (1\text{-}1)$$

and

$$\dot{\omega}(J_2) = 1.032\ (a/10{,}000\ \mathrm{km})^{-7/2}\ (4-5\sin^2 i)(1-e^2)^{-2}\ \mathrm{deg/day} \qquad (1\text{-}2)$$

For the HALCA orbit, $\dot{\Omega}(J_2) \approx -0.62$ deg/day and $\dot{\omega}(J_2) \approx 0.96$ deg/day. Thus, the precession periods for Ω and ω range between 1 and 1.7 years, less than the mission lifetime of several years. This implies good imaging capability for most

sources at some time during the VSOP mission. It is useful to note that $\dot{\omega} = 0$ if $i = 63.4°$, which can be used to maximize tracking time by keeping perigee in the south (see Section 3.3).

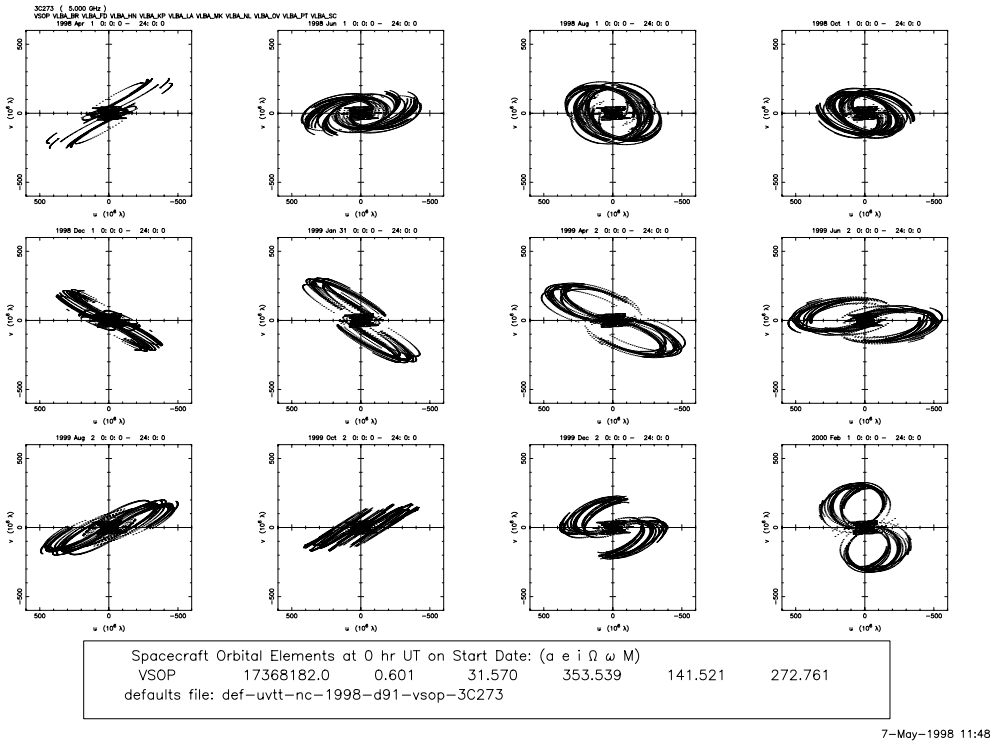

Figure 3. 5-GHz SVLBI (u,v) coverages of 3C 273 at two-month intervals, for HALCA+VLBA, starting on 1 April 1998. No HALCA observing constraints are included other than the requirement that there be a line of sight between the spacecraft and a tracking station.

Figure 3 is a FAKESAT (Murphy 1995) plot of the (u,v) coverage for 3C 273 as a function of time. The coverage is plotted at two-month intervals beginning in April 1998, for an array consisting of HALCA and the VLBA. As in Figure 2, all observing constraints have been suppressed in order to highlight the effects of orbit precession. The plot shows epochs when the coverage is nearly one-dimensional (source very close to the orbit plane), epochs when the coverage is rather two-dimensional with fairly short baselines (source close to perigee or apogee directions), and epochs where the coverage is somewhat two-dimensional with longer baselines. There is never completely two-dimensional coverage with the longest baselines, since 3C 273 is never more than 35° from the orbit plane.

3 The Space Radio Telescope

3.1 What is the "Space Radio Telescope"?

One simple way of thinking of a VLBI telescope is that it is a system consisting of five major elements or subsystems:

- Observing antenna, feed, and receivers
- Frequency converters, filters, and IF data processors
- Digitizers and samplers
- Time and frequency standard
- Formatter and wideband VLBI data recorder(s)

At ground observatories, the elements listed above are co-located, within a few tens of kilometers or less. However, in SVLBI, some subsystems are located on the spacecraft, while others are at a ground tracking station. For example, in the TDRSS experiments, only the first two subsystems were in space, while the others were located at the White Sands Ground Terminal. For VSOP, the first three subsystems are aboard HALCA, while the frequency standard and data recorders are at the tracking stations. Future missions may employ space-borne hydrogen maser clocks, although ground-based frequency standards still may be required for a variety of purposes. The combination of the five fundamental subsystems at the orbiter and the tracking station(s) is defined here as the "Space Radio Telescope." A simple block diagram, including additional elements required to connect the spacecraft to the ground, is shown in Figure 4.

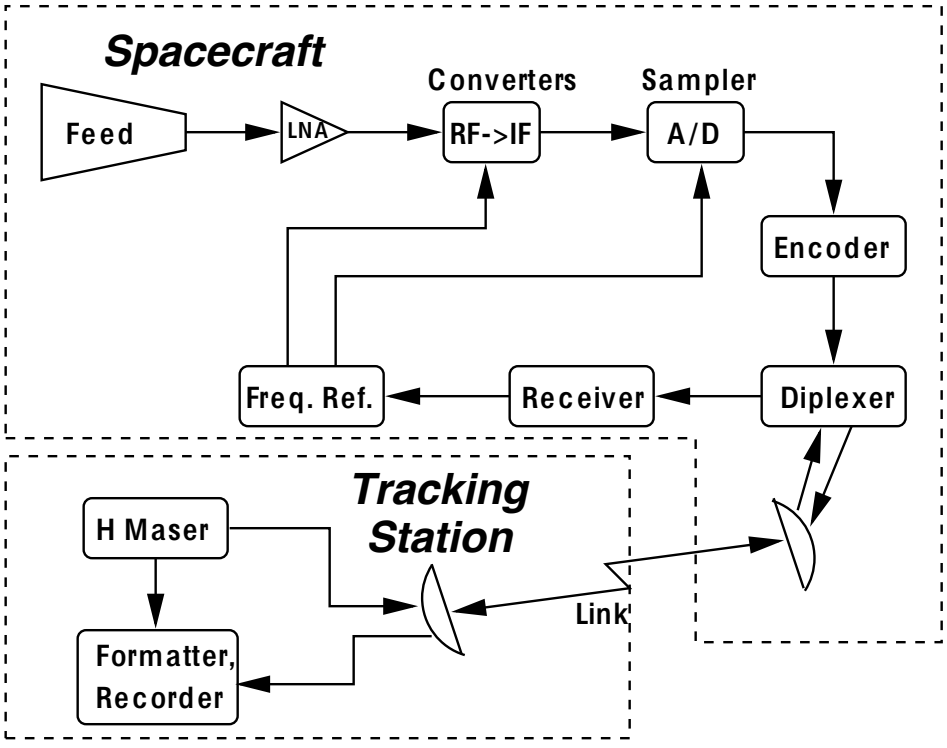

Figure 4. Simple block diagram of a generic Space Radio Telescope, consisting of an orbiting VLBI satellite and a tracking station.

Wideband VLBI data cannot be accumulated and stored aboard a spacecraft during an observation, so they must be recorded on the ground in real time. Therefore, good sampling of the (u,v) plane requires a network of tracking stations distributed around the Earth. At a given time, the Space Radio Telescope may be defined to be the orbiter and a particular tracking station, while the Space Radio Telescope for an entire scientific observation might be defined as the combination of the spacecraft and all the tracking stations that participate in that observation. The difference between the two definitions is not fundamental; the important point is that there is no operational Space Radio Telescope unless the orbiter is observing a source *and* has a reliable link with a tracking station.

3.2 The Spacecraft

The SVLBI orbiter is the "front end" of the Space Radio Telescope. General properties of the spacecraft (mass, power, attitude control, etc.) can be found elsewhere (e.g., Kardashev 1997; Hirabayashi 1998; VSOP Science Operations Group 1998; Hirabayashi et al. 1998). The critical element of the science payload is the receiving antenna, which typically works at centimeter wavelengths and is up to 10 meters in diameter; details of the design of the HALCA antenna can be found in Natori et al. (1994) and Takano et al. (1994). The receivers and IF processing subsystem are also necessary ingredients aboard the spacecraft, but are not described here, since they are fundamentally similar to the subsystems found at ground observatories. Cooling of the receivers has not been practical to date due to mass and power considerations, but is planned for the second generation of missions, VSOP-2 and ARISE (see Section 6).

3.3 Tracking Stations

Tracking stations are necessary to record the VLBI data and (so far) to provide the stable frequency reference for the spacecraft. In the case of VSOP, five tracking stations are employed, in California, West Virginia, Spain, Japan, and Australia. Four are located in the northern hemisphere, so the tracking and (u,v) coverage are much better when HALCA has apogee in the north ($0° < \omega < 180°$), and somewhat degraded when the orbit has precessed so that apogee is in the south.

The primary functions of the tracking stations are to provide a stable frequency reference, derive the correct time at which data samples were received aboard the spacecraft, provide the data necessary for accurate orbit determination, and record the wideband VLBI data. Details of the design of a tracking station are beyond the scope of the present article, but some relevant information can be found in D'Addario (1991) and in Kawaguchi et al. (1994). A separate "command" station also may be used to send commands and receive housekeeping telemetry from the spacecraft.

3.4 Timing and Data Link

In ground VLBI observations, the clock, recorder, and receiving antenna are co-located, making it relatively straightforward to time-tag the data. However, in the Space Radio Telescope (see Figure 4), this is not the case. The TDRSS experiments pioneered a method of "time transfer" (or "phase transfer") in

which a ground frequency standard was used as the reference for the VLBI subsystems in space (e.g., Levy et al. 1989).

Many details of time transfer in orbiting VLBI are described by D'Addario (1991), and are only summarized here. On the ground, a pure frequency tone referenced to a hydrogen maser clock is generated and uplinked to the spacecraft. A predicted spacecraft orbit is used to calculate the Doppler shift, and the emitted frequency of the uplink tone is varied to cause a constant frequency to be received at the spacecraft. There, the tone is received, detected, and locks a frequency reference that is used to operate the on-board oscillators. The tone also is transponded to a different frequency and re-transmitted to the ground tracking station. On the ground, the received tone is mixed with the frequency expected for the predicted Doppler shift. The residual frequency (received minus expected) is measured by a quadrature phase detector at a high rate, and the phase residual is recorded for later use.

If the predicted Doppler shift for the spacecraft is error-free, and there are no other signal delays, the phase residual will be zero, implying that the spacecraft clock was running at the correct rate. However, errors in the predicted orbit cause the residual to be nonzero. This implies that the spacecraft clock rate was in error, and that the digital data were sampled at incorrect intervals, which must be corrected in data correlation (see Section 4.2). Only the uplink (one-way) error affects the spacecraft timing, but the tracking station measures a two-way residual, which must be converted to the time error for the spacecraft.

The digitized VLBI data are downlinked in a series of telemetry frames, each led by a header containing auxiliary information about the spacecraft and its science payload. These wideband data are demodulated on the ground and recorded on digital tape in a format similar to that used by the ground radio telescopes. (In order to prevent spurious correlations, the header data are replaced by pseudo-random noise before recording.) The rate of data recording is derived from a clock driven by the downlink telemetry, not by the ground hydrogen maser. This "data clock" runs at a variable rate in the ground frame, depending on the Doppler shift imposed by the spacecraft motion. The absolute offset of the data clock from the ground clock also must be measured at some initialization epoch, to enable VLBI correlation.

The example of VSOP is the best way to illustrate the activities necessary for correct data recording and timing. A (more-or-less) chronological sequence of activities is listed below:

- Tracking station uplinks a tone to the spacecraft, with frequency varied so as to achieve a received frequency of exactly 15.3 GHz aboard HALCA.

- Spacecraft receives uplink tone and uses it to lock all local oscillators.

- VLBI data are sampled and digitized on the spacecraft at 128 Mbit $\sec^{-1}$ (two 16-MHz channels, each with 2-bit sampling), as controlled by the clock running at a constant rate in HALCA's rest frame.

- Received frequency is transponded to 14.2 GHz in the spacecraft frame, and re-transmitted to the ground tracking station along with the wideband VLBI data, which are divided into frames 80 kilobytes in length.

- Tracking station detects the downlink signal, extracts the Doppler-shifted tone, mixes it with the expected received frequency, and measures the residual phase hundreds or thousands of times per second.
- Tracking station detects valid telemetry and sets the VLBI formatter clock. Header data are diverted into a separate data file for later use. For 4 of the 5 VSOP tracking stations, the clock is set to an integer second at the start of a telemetry frame. Offset of the formatter clock from the ground hydrogen maser clock is recorded for future reference.
- Wideband data are demodulated from the downlink and recorded on a VLBI tape for supply to the designated correlator. After initialization, the clock rate is governed by the data clock, with 128 Megabits defining one "second" (differing from a ground "second" by the Doppler shift).
- Two-way phase residuals are recorded throughout the tracking pass, at rates of 400 Hz or higher.

After a tracking pass, a "Time Corrections File" is generated, containing the information needed to relate the time on the VLBI tape to the time that a data sample was received aboard HALCA. This file incorporates the following:

- Clock initialization offset.
- Timing error derived from the measured round-trip phase residual.
- Additional delays in the tracking station hardware.
- Geometric delay (light travel time) on the downlink from spacecraft to tracking station.
- Any other effects considered significant at the tracking station.

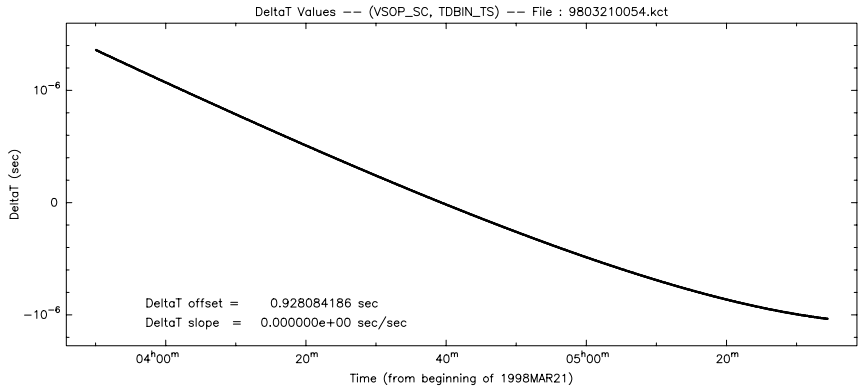

Figure 5. Time Corrections File for Tidbinbilla tracking of HALCA, from 03:50 to 05:35 UT on 21 March 1998. The range of corrections is slightly larger than ± 1 μsec.

The Time Corrections File is supplied to the VLBI correlators for use in the final correlation (see Section 4.2). Figure 5 shows a portion of the Time

Corrections File from the Tidbinbilla (Australia) tracking station for a 5-GHz VSOP observation of 3C 345, on 21 March 1998. In this plot, a constant delay offset has been removed. The variation in the clock error over 1.75 hr is about 2.4 μsec, more than 10,000 cycles at the observing wavelength of 6 cm. (The speed of light, in convenient units, is 30 cm nsec^{-1}, so a 1-nsec shift corresponds to 5 wavelengths.) If this clock correction was not applied in correlation, the coherence would be severely degraded (see Section 4.4 and Figure 8).

3.5 Orbit Determination

Orbit determination for SVLBI uses the same data from which the time corrections are derived (see Section 3.4). These data are measurements of the two-way Doppler shift, which can be used to derive the spacecraft orbit. (In addition, range and Doppler measurements may be made from the command station.) The spacecraft orbit is derived using a detailed model of the Earth's gravitational field as well as a solar-pressure model for the spacecraft, taking into account the pointing direction of the large radio antenna. Uncertainties in the gravitational field are especially important if the spacecraft has a low perigee height. Solar-pressure effects are more important than for most spacecraft, because the large radio telescope leads to a high area/mass ratio for the spacecraft.

For HALCA, the orbit determination typically provides reconstructed orbits for VLBI correlation that have r.m.s. position and velocity accuracies of about 15 m and 6 mm sec^{-1}, respectively. These accuracies are good enough for VLBI correlation, but not for global astrometry. Orbits predicted a few days in advance are typically several times less accurate. Second-generation SVLBI missions will make use of Global Positioning System (GPS) receivers aboard the spacecraft, providing position accuracies predicted to be better than 10 cm over the entire orbit.

3.6 Observing Constraints

There are a variety of constraints on observing with a Space Radio Telescope that differ from a ground telescope. There are Sun-angle constraints caused by the necessity to point the spacecraft solar panels at the Sun, requirements to shade parts of the spacecraft from direct sunlight, and limited reaction-wheel capacity to remove torques imposed by solar radiation pressure. Communication constraints include the requirement that a tracking station be able to view the spacecraft, as well as the requirement that the spacecraft telemetry antenna have a clear line of sight to that tracking station. The latter requirement may be violated because of blockages on the spacecraft that depend on observation direction. In addition, there are eclipse constraints, since power and thermal requirements normally will prevent observations during (or near) times when the Sun is eclipsed by either the Earth or the Moon. Finally, there are miscellaneous constraints related to issues such as command-storage capability and spacecraft slew rates. Slew-rate limitations, for instance, make phase-referencing VLBI observations (Beasley & Conway 1995) difficult or impossible for any realistic spacecraft design.

Descriptions of VSOP constraints in some detail can be found in the VSOP Proposers Guide (VSOP Science Operations Group 1998); their effect is illustrated in Figures 6 and 7. Figure 6 is the all-sky (u,v) coverage for HALCA and

the VLBA on 1 April 1998, similar to Figure 2, but now including all relevant constraints on VSOP observing. Note the large exclusion zones in Figure 6 due to source proximity to the Sun. Similarly, Figure 7 is a repetition of Figure 3, a plot of the (u,v) coverage for 3C 273 every two months, with all constraints now included. There are long periods for which no SVLBI observations of 3C 273 are possible, because the source is near the ecliptic plane and is too close to the Sun for about five months per year. These constraints and the variable (u,v) coverage make SVLBI scheduling fairly complex (e.g., Meier 1998).

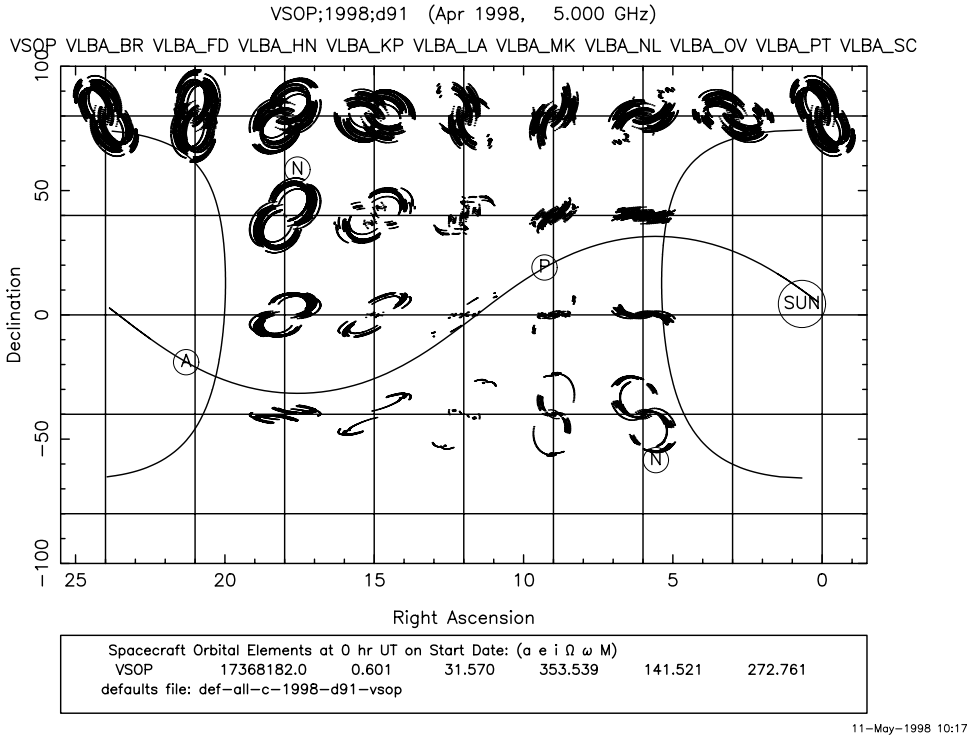

Figure 6. 5-GHz SVLBI (u,v) coverages as a function of sky position, for HALCA+VLBA, on 1 April 1998, including all observing constraints on the Space Radio Telescope. (Compare to Figure 2.)

3.7 Data Calibration

Calibration of the Space Radio Telescope is somewhat different from a ground telescope, and depends on downlink telemetry from the orbiter (see Section 3.4). Because of command-storage constraints, it may be impossible to fire a noise diode regularly. Also, ground telescopes often incorporate several different noise diodes of differing strengths, but power and mass constraints may prevent this for a spacecraft. For example, aboard HALCA, the only available noise diode approximately doubles the system noise temperature. Therefore it is not beneficial to use the noise source during VLBI observations, since it would significantly increase the system noise temperature.

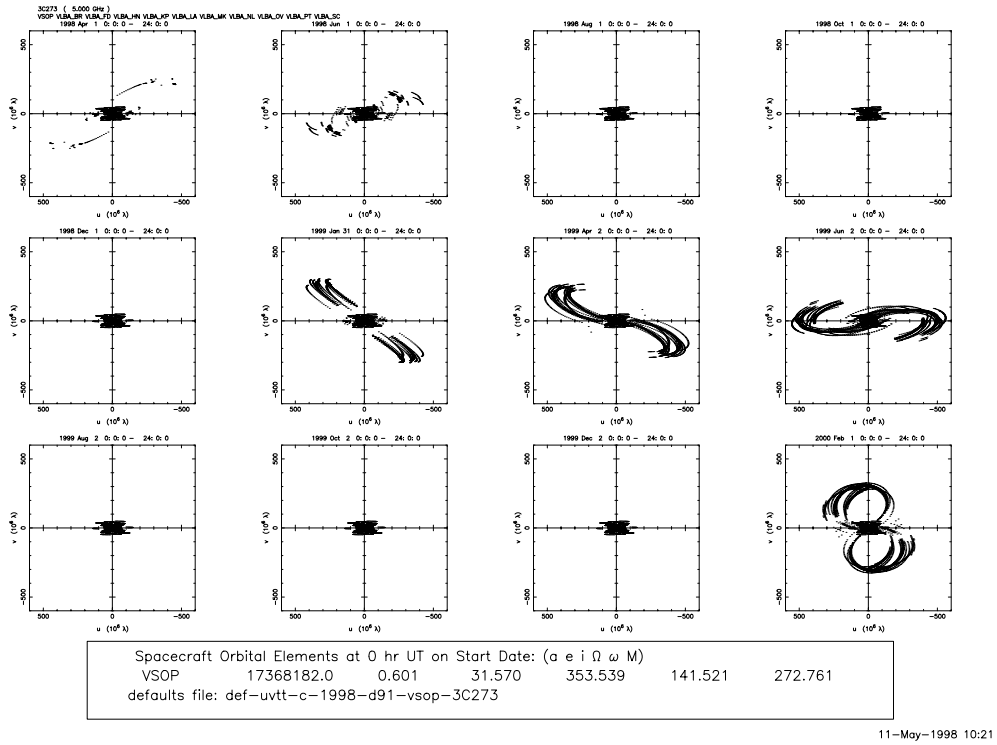

Figure 7. 5-GHz SVLBI (u,v) coverages of 3C 273 at two-month intervals, for HALCA+VLBA, starting on 1 April 1998, including all observing constraints on the Space Radio Telescope. (Compare to Figure 3.)

The low sensitivity and constraints on observing directions also make it difficult to calibrate the pointing using observations of strong radio sources. This can be especially troublesome because the pointing offsets may change substantially as a function of Sun angle. For HALCA, the uncertain pointing calibration made it difficult to attempt fringe detection with the 22-GHz system, which was damaged during launch and has extremely poor sensitivity. (These fringe searches were ultimately successful thanks to a huge flare in the Orion H_2O maser.)

A great advantage in calibration of the Space Radio Telescope is the lack of an atmosphere above the spacecraft. For HALCA, the system temperature shows good repeatability from orbit to orbit, at the level of about 2%. Variations within an orbit may be as large as 5% due to changing thermal conditions near eclipses. However, even these changes are relatively consistent for adjacent orbits, so they can be calibrated by using measurements made on orbits before or after the actual observations. In fact, experience has shown that the system temperature calibration for HALCA is considerably more accurate than for some of the ground radio telescopes involved in VSOP observations.

Polarization calibration of SVLBI data is also rather difficult due to the low signal-to-noise ratio. HALCA observes only in a single polarization (left circular), and the lack of rotation of the parallactic angle makes calibration of the polarization leakage terms rather involved. However, such calibration

has been carried out successfully by the VSOP Polarization Study Team as part of in-orbit checkout (Kemball et al. 1998). Polarization calibration for missions with dual polarization and higher sensitivity might be easier, but the off-axis antenna designs under consideration for some future missions will lead to additional complications.

4 Correlation and Data Processing

The VLBI correlation process is described in some detail by Romney (1995), with the actual implementation at the VLBA correlator discussed by Benson (1995). Those discussions are not repeated here. Instead, we concentrate on the fundamental differences and additions that are necessary for SVLBI.

4.1 Delay Model

VLBI correlation requires an accurate delay model for each instant of an observation. The delay model is a representation of the apparent delay in the wavefront received at a radio telescope, typically referred to its arrival time at the Earth's center, and includes many different effects on the signal, as well as the models of the observatory clocks. The data are referenced to the delay model so that the interference fringes are "stopped," and the residual delays and delay rates are small. Small residuals enable long coherent integrations in fringe-fitting, which translates into a capability for detecting fringes on weaker sources.

In ground VLBI, the geometric part of the delay (τ_g) is always negative (the telescope is always "in front of" the Earth's center, as viewed from the radio source), and its maximum magnitude is about 21 msec. The maximum rate of change of the geometric delay is $\leq$ 3 μsec sec^{-1}. This "fringe rate" or "fringe frequency" often is expressed in units of cycles of the observing frequency, by multiplying the delay rate by the observing frequency. For an observing frequency of 100 GHz, therefore, the maximum ground-VLBI fringe rate is $\leq$ 300 kHz.

For SVLBI, the maximum delay and fringe rate that must be accommodated are much larger. For example, if the spacecraft has an apogee height of 90,000 km, the delay of the downlink will be approximately 0.3 sec, and the geometric delay may be of the same magnitude, with either the same or the opposite sign. Furthermore, initialization offsets of the station clock relative to ground UTC (see Section 3.4) also can be on the order of a second. Both the spacecraft geometric delay and the total delay, therefore, can be either positive or negative, and have magnitudes of seconds. Fortunately, most modern correlators can accommodate unlimited delay by offsetting the tapes during playback.

The delay rate (and delay "acceleration") are more difficult to address. A rough approximation to the maximum delay rate can be made by taking the maximum spacecraft speed in an elliptical Earth orbit, $\sim$ 10 km sec^{-1}, and dividing this by the speed of light to yield a delay rate of $\sim$ 33 μsec sec^{-1}. When Earth rotation and slightly higher speeds for an extremely elliptical orbit are included, the correlator needs to accommodate a delay rate approaching 40 μsec sec^{-1}. The delay models inside VLBI correlators are usually expressed as polynomials in time that are good for a limited time interval, and are further approximated as linear functions over a shorter interval (see Benson 1995). Therefore, the higher

SVLBI delay rate may require more accurate polynomial fitting and evaluation, more frequent model updates, and even additional hardware.

4.2 Correlator Inputs

Achievement of an accurate delay model requires that the observation geometry and the clock models be well specified, so the correlator can correctly process the digitized VLBI data. For a ground telescope, inputs include an accurate telescope location, a precise Earth-rotation model (including polar motion), an accurate radio-source position, and a measurement of the observatory clock error relative to some fiducial UTC reference, such as the network of GPS satellites. These models and measurements are relatively simple to input, consisting of just a few numbers.

For SVLBI, there are two crucial complications. First, the position of the telescope is not tied to the Earth's surface, but is a much more complicated function. A detailed orbit ephemeris is typically provided as a six-dimensional (position and velocity) spacecraft state vector as a function of time; this ephemeris is used to generate the geometric delay model. Second, the clock model must be represented by a Time Corrections File (see Section 3.4). This file contains the information necessary to correct for clock errors imposed by the process of "constructing" the Space Radio Telescope. For VSOP, the Time Corrections File is supplied as a series of 10 corrections per second, which are added to the time on the VLBI tape in order to specify the time at which a data sample was acquired. The high frequency of these corrections was specified to guard against changes in the atmosphere or electronics at frequencies as high as 5 Hz, which would cause coherence loss if not properly sampled. Actual experience has shown that fitting a high-order (5th order in time) polynomial to the Time Corrections File every 10 seconds causes no significant loss of coherence. Use of such a polynomial makes correlator implementation simpler, since it can be added to the other components of the delay polynomial (with the appropriate sign!) in generating the correlator model.

Two important input parameters for VLBI correlation are the window sizes for the output residual delay and fringe rate. Standard parameters for ground VLBA observations are about ± 4 μsec for the delay, and ± 0.25 Hz for the fringe rate. The r.m.s. position error of HALCA (see Section 3.5) corresponds to less than 100 nsec in delay, so once the constant offsets are determined for a tracking station, it is possible to correlate spacecraft data without increasing the residual delay window. A velocity error of ± 1 cm sec^{-1} corresponds to a fringe-rate error of ± 0.17 Hz for an observing frequency of 5 GHz, not much smaller than the typical ground-only fringe-rate window. Therefore, at the VLBA correlator, the space-ground baselines of a 5-GHz VSOP experiment are typically output with a 1.04-sec integration time, corresponding to a residual rate window of ± 0.48 Hz. This increases the output data rate significantly; in order to keep the sizes of output data sets manageable, SVLBI correlators typically have (and use!) the capability of outputting the ground-ground baselines less frequently than the space-ground baselines.

4.3 Fringe-fitting

Fringe-fitting of SVLBI data has some important distinctions from the process used for ground VLBI data. First, the sensitivity of the Space Radio Telescope is quite low compared to most ground telescopes. Second, because the spacecraft cannot slew rapidly, it is not possible to observe strong calibration sources, so the program source provides the only option for locating the space-ground fringes. Third, location of fringes for the Space Radio Telescope is dependent on the accuracy of the orbit and of the Time Corrections File, so the initial searches often must employ wider search windows than for ground VLBI.

In order to assess the likelihood of detecting fringes, and the limitations on the source strength that can be detected for a given SVLBI mission, we use the following formula for the r.m.s. noise (ΔS_{ij}) for a weak source on a single baseline between antennas i and j, in a fringe-fit interval $\tau_{\rm acc}$ (e.g., Crane & Napier 1989; Wrobel & Walker 1998):

$$\Delta S_{ij} \;=\; \frac{\sqrt{T_{{\rm sys},i}\; T_{{\rm sys},j}}}{C\eta_s\sqrt{(2\;\Delta\nu\;\tau_{\rm acc}\;K_i\;K_j)}}\;. \qquad (1\text{-}3)$$

Here, $K_i = (\eta_{a,i}A_i)/(2k_B)$, where $\eta_{a,i}$ is the aperture efficiency of antenna i, A_i is its physical area, and k_B is Boltzmann's constant. In addition $T_{{\rm sys},i}$ is the system temperature of antenna i; C is the coherence ($C \equiv 1$ for perfect coherence); η_s is the system efficiency factor (due to 1- or 2-bit sampling, fringe rotator quantization, etc.); and $\Delta\nu$ is the observing bandwidth.

Often, we express the sensitivity of a telescope in jansky by dividing its system temperature (in K) by its gain (in K/Jy), to derive a quantity known as the "System-Equivalent Flux Density" (SEFD). Then,

$$\mathrm{SEFD}_i \;=\; \frac{T_{{\rm sys},i}}{K_i}\;, \qquad (1\text{-}4)$$

and

$$\Delta S_{ij} \;=\; \frac{\sqrt{\mathrm{SEFD}_i\;\mathrm{SEFD}_j}}{C\eta_s\sqrt{2\;\Delta\nu\;\tau_{\rm acc}}}\;. \qquad (1\text{-}5)$$

Fringe detection requires a signal-to-noise ratio of approximately 7 to minimize the probability of a false detection (see Thompson, Moran, & Swenson 1986, pp. 259–269); i.e., the minimum correlated flux density of the target source must be $S_{\rm c,min} \geq 7\Delta S_{ij}$. As an example, we compute $S_{\rm c,min}$ for two 25-m VLBA antennas at 5 GHz, assuming a 300-second integration over a 16-MHz bandpass, with 2-bit sampling. For these antennas, SEFD ≈ 300, and $\eta_s = 0.88$ for 2-bit sampling, so $S_{\rm c,min} \geq 24$ mJy. However, for SVLBI, the space telescope is usually much less sensitive than a ground telescope. In particular, the 5-GHz SEFD of HALCA is approximately 16,000 Jy, so $S_{\rm c,min} \geq 180$ mJy.

A variety of fringe-fitting techniques have been investigated in processing VSOP data. Accurate amplitude calibration is helpful, so that global fringe-fitting programs can give appropriate weight to the strongest baselines. Parameters in the AIPS task FRING enable different methods of combining or "stacking" the baselines in the fringe search, which can improve the detection threshold by critical factors of 1.5–2. Restricting the size of the fringe-search

window is often important, since this limits the number of cells that must be searched, reducing the strength of the largest noise spike expected. Finally, it is sometimes useful to set a very low signal-to-noise threshold in order to accept all FRING solutions; the residual delays and rates can be plotted to search for repeating values, which may indicate the presence of weak fringes.

4.4 Coherence

It is desirable to use the longest possible integration time, $\tau_{\rm acc}$, in fringe fitting, as long as the coherence $C \approx 1$ (see Equation 1-5). For VSOP, coherence times of $\tau_c \approx$300–400 seconds are typical at 5 GHz, while τ_c may be 500–600 seconds at 1.6 GHz. (Here, τ_c is defined to be the interval over which C falls to 0.9.) These are in good agreement with the values predicted prior to launch, based on the expected orbit accuracy, propagation effects in the Earth's atmosphere, and the properties of the phase-transfer process. Coherence times at both frequencies are often reduced by factors of 2–4 within 30–60 minutes of perigee, apparently due to increased errors in the reconstructed velocity at low altitudes. We note the dependence of the coherence on the r.m.s. phase residual, $\Delta\phi_{\rm rms}$:

$$C = 1 - \frac{(\Delta\phi_{\rm rms})^2}{2} \ . \qquad \text{(1-6)}$$

After a delay which is a linear function of time has been fitted and removed, if the time derivative of the residual fringe rate is defined as $\dot{\nu}_0$, the integration time for 90% coherence can be shown to be

$$\tau_c \approx 375 \left(\frac{\dot{\nu}_0}{10 \text{ mHz hr}^{-1}} \right)^{-1/2} \text{ sec} \ . \qquad \text{(1-7)}$$

Figure 8 shows the impact of the Time Corrections File on the fringe-fit residuals and coherence for a 5-GHz VSOP observation of 3C 345, on 21 March 1998. The top panels show the residual delay and fringe rate for the Space Radio Telescope in correlation of a 1.75-hr segment of the observation without use of a Time Corrections File, from 03:50 to 05:35 UT. (For reference, note that perigee was at 06:09 UT.) The fringes were centered at the initial time by extracting a constant clock offset from the Time Corrections File; otherwise no fringes could have been found. The residual fringe rate approaches the maximum value of $\pm$3.8 Hz for the VLBA correlator, and the change in that rate ranges from $\sim$ 300 mHz hr^{-1} near 04:00 to $\sim$ 1100 mHz hr^{-1} near 05:30. Equation 1-7 then implies coherence times ranging from 35 to 70 sec. The bottom panel shows the results of a correlation of the same data set using the Time Corrections File, which was shown previously in Figure 5. Note that the ranges of residual delay and fringe rate are both reduced by more than two orders of magnitude, The maximum variation of the residual rate is $\sim$ 10 mHz hr^{-1}, implying $\tau_c \approx$ 375 sec. This increase in τ_c by a factor of $\sim$ 9 causes the noise to be reduced by a factor of $\sim$ 3, which can enable detection of SVLBI fringes for many more sources. The residual rate after application of the Time Corrections File, which corresponds to a velocity of about 1 mm sec^{-1}, is almost surely due to the effect of orbit errors on the interferometer model.

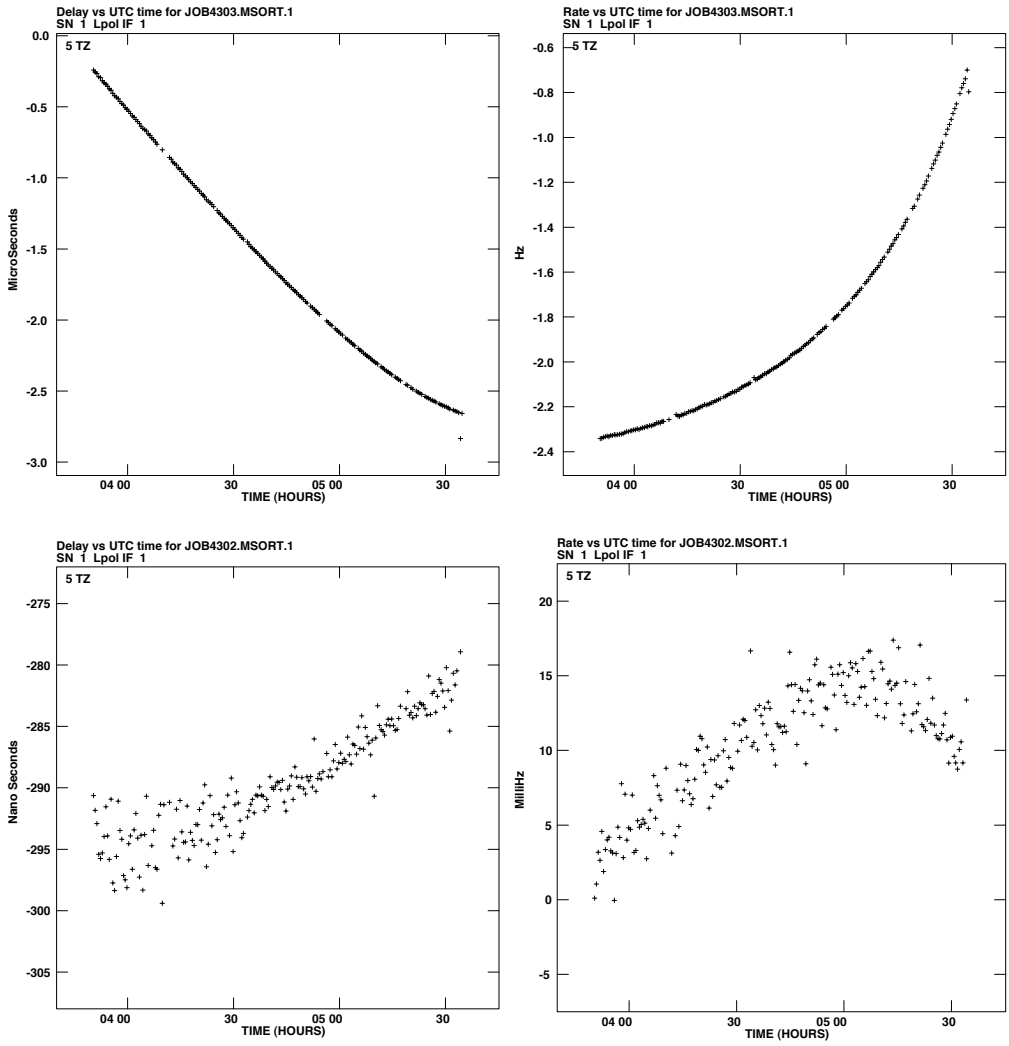

Figure 8. Residuals to fringe fits for a 5-GHz observation of 3C 345 using HALCA and the Tidbinbilla tracking station. Residual delays are on the left, and residual fringe rates on the right. *Top:* Results for correlation without a Time Corrections File. *Bottom:* Results for correlation using the Time Corrections File shown in Figure 5.

5 Imaging and Modeling

It has taken many years to establish imaging and model-fitting techniques for ground VLBI. Scientific data from VSOP have been available for only a year, and we are just learning the best procedures to use for SVLBI. Imaging is typically done using DIFMAP (Shepherd 1997) in the Caltech VLBI package, or either IMAGR or SCMAP in AIPS (van Moorsel, Kemball, & Greisen 1996). This section will be limited to somewhat general comments; major progress is expected over the next several years.

5.1 Data Weighting

Data weighting during fringe fitting depends on the sensitivity of the individual baselines, as derived from the *a priori* calibration. In imaging, one can use weighting ranging from purely "natural" (equal weight for each visibility point) to purely "uniform" (equal weight for each grid cell); Briggs (1995, 1998) describes a "robustness" parameter that can be used to adjust the weights between the two extremes. It is also possible to "taper" the data, giving higher weight to the shorter projected baselines. In SVLBI, in order to achieve the highest resolution, it is desirable to give a high weight to the baselines involving the orbiting antenna. Therefore, natural weighting and significant tapering are generally undesirable, since both will down-weight the space baselines and make the final image approach that from a ground-only VLBI observation.

5.2 Self-Calibration

Self-calibration is a critical element of SVLBI. Sampling of the (u,v) plane is poorer than for the VLBA, particularly for southern sources observed with sparse ground arrays. Often, the sampling leads to a dirty beam with sidelobes as high as 30%–50% of the main beam, so calibration errors will scatter large amounts of flux around the map. The spacecraft typically is at the end of many similar long baselines, so the closure phase used in phase self-calibration is poorly constrained (Linfield 1986). Some observations include only 3 or 4 ground telescopes with relatively poor *a priori* calibration. Phase self-calibration (requiring groups of 3 telescopes) and amplitude self-calibration (requiring 4 telescopes) may not be very effective in improving images for these small ground arrays.

Careful data editing is more important for SVLBI than for the VLBA because of the difficulties with self-calibration. In particular, tracking stations may have delay jumps or multiple clock initializations. It is important to identify these events, and either flag the data or break the fringe fits at appropriate times. One technique used by the author is to perform amplitude self-calibration with a short solution interval (minutes), inspect the solutions for large corrections to the spacecraft gain, and use this to identify data that should be flagged before performing the "real" self-calibration.

An important aspect of self-calibration is to start off with some knowledge of the structure of the program source. Even simple information about the jet direction helps greatly; otherwise, large sidelobes may make it difficult to distinguish real structures from spurious components, and self-calibration will not easily remove false symmetries. Most of the strong sources observed by HALCA have been imaged at 2.3 and 8.5 GHz (Fey, Clegg, & Fomalont 1996), and the on-line images (*http://maia.usno.navy.mil/rorf/rrfid.html*) can be extremely valuable. Ground-based VLBA images at 15 GHz (Kellermann et al. 1998; see *http://www.cv.nrao.edu/2cmsurvey/*) also are quite useful.

5.3 Dynamic-Range Limitations

It is difficult to quantify the dynamic range possible for SVLBI observations. For HALCA observing with the VLBA, dynamic ranges (the ratio of the peak flux density to either the average map noise or the strongest spurious feature) of a few hundred have been achieved with moderately good sampling of the (u,v) plane (see Section 5.4). On the other hand, for VSOP survey observations

involving only 2–3 ground telescopes, dynamic ranges of only 10–20 may be achievable. For these data, model-fitting in the (u,v) plane may be the best way of characterizing the source. Classical model-fitting techniques weight the data by the baseline sensitivities, but this gives low weight to the space baselines, hardly a desirable circumstance. Since the techniques of SVLBI model-fitting are still poorly explored, no further details will be given here.

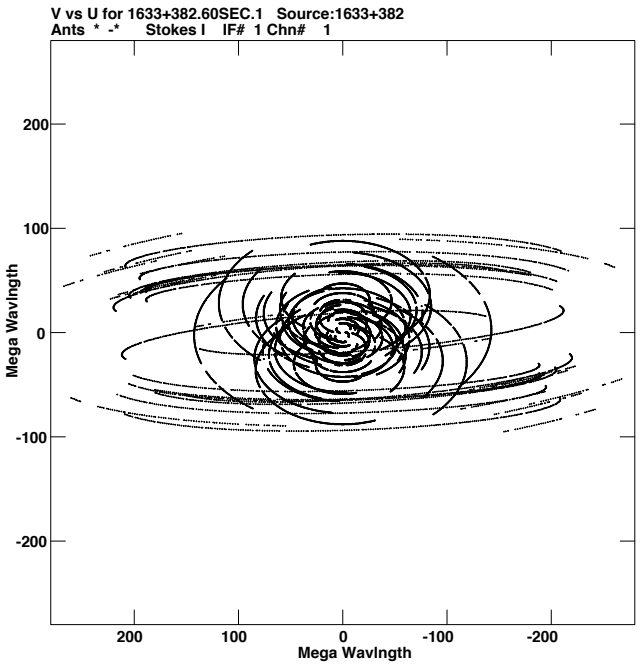

Figure 9. (u,v) coverage for HALCA+VLBA observations of 1633+382 on 29/30 July 1997.

5.4 Sample Image

A VSOP observation of the γ-ray blazar 1633+382 (Ulvestad et al. 1998) can be used to illustrate the results of SVLBI imaging. This source was observed at 5 GHz by HALCA and the VLBA during the VSOP in-orbit checkout, on 29/30 July 1997. The ground telescopes spent about 9 hr on source, while 5 hr of useful HALCA data were supplied via the tracking stations in West Virginia and California. The (u,v) coverage for this observation is shown in Figure 9; the projected baseline lengths were less than half the maximum achievable for VSOP. Therefore, the (u,v) plane was well filled, giving good imaging capability, but sub-optimal resolution. In fact, the North-South resolution was not much better than that of the VLBA, while the East-West resolution was a factor of ~ 2 better than for the ground-only array.

Two resulting images of 1633+382 are shown in Figure 10. The left-hand panel shows the ground-only image, while the right-hand panel shows the image made including HALCA. In this case, the improvement in the East-West resolution was critical for separating the central source into two distinct components. The dynamic range of the VSOP image is several hundred to one.

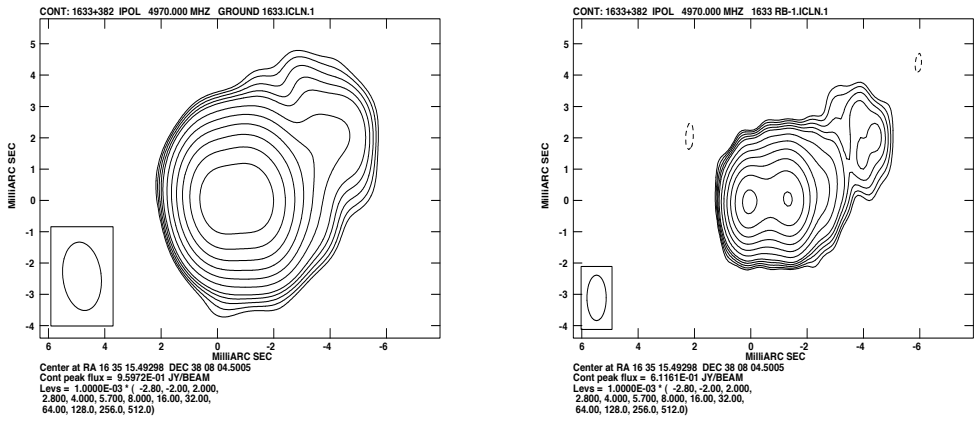

Figure 10. Two 5-GHz images of γ-ray blazar 1633+382, at identical scales, from data taken on 29/30 July 1997. *Left:* ground image, using only the VLBA telescopes. *Right:* SVLBI image, using the VLBA and HALCA.

6 Future Missions

6.1 RadioAstron

RadioAstron (Kardashev 1997) is a first-generation SVLBI mission being developed under the leadership of the Astro Space Center in Moscow. The RadioAstron launch was scheduled to precede HALCA's launch, but financial problems have delayed it until after the turn of the millennium. RadioAstron will carry a 10-m radio telescope that is planned to operate in four frequency bands: 0.3, 1.6, 4.8, and 22.2 GHz. The nominal orbit is a 28-hr orbit with an apogee height of nearly 80,000 km and an initial perigee height of 4,000 km, although there also has been talk of a 4-day or even an 8-day orbit. RadioAstron will use a set of tracking stations similar to those available for VSOP, but with a station in Russia replacing the station in Japan. The link frequency for the tracking stations will be 8 GHz rather than the 15-GHz frequency used for HALCA, so ionospheric effects on the link may reduce the coherence slightly.

6.2 VSOP-2

VSOP-2 is a possible successor to VSOP. A formal working group has been formed at ISAS, and a proposal for a new start for VSOP-2 is expected in 1999 or 2000. If the mission is approved, the launch date would be about 2006 or later. The VSOP-2 spacecraft would have an orbit similar to VSOP, with a 10-m antenna, cooled receivers, frequency coverage up to 43 GHz, and a data rate of about 1 Gbit sec^{-1}. Therefore, the interferometer sensitivity of VSOP-2 would be about 10 times better than VSOP.

6.3 ARISE

ARISE (Advanced Radio Interferometry between Space and Earth) is a mission concept currently being studied within NASA's Structure and Evolution of the Universe theme. It is in the long-term "roadmap" for that theme, with a possible

launch envisioned in 2008 or later. ARISE is an ambitious mission concept, whose basic goal is to launch a VLBA-equivalent telescope into an elliptical orbit with an apogee height of roughly 40,000 km. The telescope would be a 25-m inflatable antenna with cooled receivers, frequency coverage as high as 86 GHz, and a data rate of 1–8 Gbit sec^{-1}. Further details on this mission concept can be found in a number of references (e.g., Gurvits, Ulvestad, & Linfield 1996; Ulvestad, Gurvits, & Linfield 1997; Ulvestad & Linfield 1998).

Acknowledgments. I thank the many participants in the international Space VLBI endeavors for their efforts, David Murphy for development and distribution of the FAKESAT software, and Mark Claussen and Phil Edwards for reviewing earlier drafts of this chapter. Special gratitude is due to Gerry Levy, who pioneered Space VLBI by making the TDRSS experiments happen, and to Roger Linfield, for years of collaboration and discussions on all aspects of Space VLBI. Space VLBI efforts at NRAO are funded by the National Aeronautics and Space Administration.

References

Bate, R. R., Mueller, D. D., & White, J. E. 1971, *Fundamentals of Astrodynamics,* (New York: Dover).

Beasley, A. J., & Conway, J. E. 1995, in *Very Long Baseline Interferometry and the VLBA*, ASP Conf Series 82, eds. J. A. Zensus, P. J. Diamond, & P. J. Napier (San Francisco: ASP), 327–343.

Benson, J. M. 1995, in *Very Long Baseline Interferometry and the VLBA*, ASP Conf Series 82, eds. J. A. Zensus, P. J. Diamond, & P. J. Napier (San Francisco: ASP), 117–131.

Boden, D. G. 1992, in *Space Mission Analysis and Design,* 2nd edition, eds. W. J. Larson & J. R. Wertz (Torrance, CA: Microcosm, Inc.), Chapter 6.

Bridle, A. H., & Schwab, F. R. 1989, in *Synthesis Imaging in Radio Astronomy*, ASP Conf Series 6, eds. R. A. Perley, F. R. Schwab, & A. H. Bridle (San Francisco: ASP), 247–258.

Briggs, D. 1995, *High Fidelity Deconvolution of Moderately Resolved Radio Sources,* Ph.D. thesis, New Mexico Institute of Mining and Technology.

Briggs, D. 1998, this volume.

Crane, P. C., & Napier, P. J. 1989, in *Synthesis Imaging in Radio Astronomy*, ASP Conf Series 6, eds. R. A. Perley, F. R. Schwab, & A. H. Bridle (San Francisco: ASP), 139–165.

D'Addario, L. 1991, *IEEE Trans. on Instrumentation and Measurement,* 40, 584–590.

Fey, A. L., Clegg, A. W., & Fomalont, E. B. 1996, *ApJS*, 105, 299–330.

Griffin, M. D., & French, J. R. 1991, *Space Vehicle Design* (Washington: American Institute of Aeronautics and Astronautics), Chapter 4.

Gurvits, L. I., Ulvestad, J. S., & Linfield, R. P. 1996, in *Large Antennas in Radio Astronomy,* ed. C. G. M. van't Klooster (Noordwijk: ESTEC), 81–88.

Hirabayashi, H. 1998, in *IAU Colloquium 164: Radio Emission from Galactic and Extragalactic Compact Sources*, ASP Conf Series 144, eds. J. A. Zensus, G. B. Taylor, & J. M. Wrobel (San Francisco: ASP), 11–15.

Hirabayashi, H., et al. 1998, *Science,* in press.

Hirosawa, H., & Hirabayashi, H. 1995, in *IEEE AES Systems Magazine,* June 1995, 17–23.

Kardashev, N. S. 1997, *Experimental Astronomy,* 7, 329.

Kawaguchi, N., Kobayashi, H., Miyaji, T., Mikoshiba, H., Tojo, A., Yamamoto, Z., & Hirosawa, H. 1994, in *VLBI Technology: Progress and Future Possibilities,* eds. T. Sasao, S. Manabe, O. Kameya, & M. Inoue (Tokyo: Terra Scientific), 26–33.

Kellermann, K. I., Vermeulen, R. C., Zensus, J. A., & Cohen, M. H. 1998, *AJ*, 115, 1295–1318.

Kemball, A., et al. 1998, *Polarization VLBI observations at 1.6 GHz and 5 GHz with the HALCA satellite: first results from in-orbit checkout observations,* available from *http://www.vsop.isas.ac.jp/obs/Pol.html.*

Levy, G. S., et al. 1986, *Science,* 234, 187–189.

Levy, G. S., et al. 1989, *ApJ*, 335, 1098–1104.

Linfield, R. P. 1986, *AJ*, 92, 213–218.

Linfield, R. P., et al. 1989, *ApJ*, 335, 1105–1112.

Linfield, R. P., et al. 1990, *ApJ*, 358, 350–358.

Meier, D. L. 1998, in *IAU Colloquium 164: Radio Emission from Galactic and Extragalactic Compact Sources*, ASP Conf Series 144, eds. J. A. Zensus, G. B. Taylor, & J. M. Wrobel (San Francisco: ASP), 421–422.

Murphy, D. W., et al. 1994, in *VLBI Technology: Progress and Future Possibilities,* eds. T. Sasao, S. Manabe, O. Kameya, & M. Inoue (Tokyo: Terra Scientific), 34–38.

Murphy, D. W. 1995, *BAAS,* 186, 2706

Natori, M. C., Takano, T., Miyoshi, K., Inoue, T., & Kitamura, T. 1994, in *VLBI Technology: Progress and Future Possibilities,* eds. T. Sasao, S. Manabe, O. Kameya, & M. Inoue (Tokyo: Terra Scientific), 10–20.

Pilbratt, G. 1991, in *IAU Colloquium 131: Radio Interferometry: Theory, Techniques and Applications,* ASP. Conf. Series 19, eds. T. J. Cornwell & R. A. Perley (San Francisco: ASP), 102–106.

Romney, J. D. 1995 in *Very Long Baseline Interferometry and the VLBA*, ASP Conf Series 82, eds. J. A. Zensus, P. J. Diamond, & P. J. Napier (San Francisco: ASP), 17–37.

Schilizzi, R. T., et al. 1984, in *IAU Symposium 110: VLBI and Compact Radio Sources,* eds. R. Fanti, K. Kellermann, & G. Setti (Dordrecht: Reidel), 407–414.

Shepherd, M. C. 1997, in *Astronomical Data Analysis Software and Systems VI,* ASP Conf. Series 125, eds. G. Hunt & H. E. Payne (San Francisco: ASP), 77–84.

Sramek, R. A., & Schwab, F. R. 1989, in *Synthesis Imaging in Radio Astronomy*, ASP Conf Series 6, eds. R. A. Perley, F. R. Schwab, & A. H. Bridle (San Francisco: ASP), 117–138.

Takano, T., Natori, M., Ohnishi, A., Miura, K., Inoue, T., Noguchi, T., & Kitamura, T. 1994, in *Proceedings of the 19th International Symposium on Space Technology and Science,* eds. M. Hinada, Y. Arakawa, Y. Horikawa, J. Kawaguchi, T. Nakajima, & I. Nakatani (Tokyo: Agne Shofu), 483–492.

Thompson, A. R., Moran, J. W., & Swenson, G. W. 1986, *Interferometry and Synthesis in Radio Astronomy* (New York: Wiley & Sons).

Ulvestad, J. S., Gurvits, L. I., & Linfield, R. P. 1997, in *High Sensitivity Radio Astronomy,* eds. N. Jackson & R. Davis (Cambridge: Cambridge University Press), 252–255.

Ulvestad, J. S., & Linfield, R. P. 1998, in *IAU Colloquium 164: Radio Emission from Galactic and Extragalactic Compact Sources*, ASP Conf Series 144, eds. J. A. Zensus, G. B. Taylor, & J. M. Wrobel (San Francisco: ASP), 397–398.

Ulvestad, J. S., Vestrand, W. T., Stacy, J. G., & Biretta, J. A. 1998, in preparation.

van Moorsel, G., Kemball, A., & Greisen, E. 1996, in *Astronomical Data Analysis Software and Systems V,* ASP Conf. Series 101, eds. G. H. Jacoby & J. Barnes (San Francisco: ASP), 37–43.

VSOP Science Operations Group 1998, *AO2 Proposers Guide, VLBI Space Observatory Program,* ed. D. W. Murphy, available from http://www.vsop.isas.ac.jp.

Walker, R. C. 1984, in *Indirect Imaging,* ed. J. A. Roberts (Cambridge: Cambridge University Press), 53–65.

Wrobel, J. M., & Walker, R. C. 1998, this volume.